# Gravity-Assist Low-Thrust Inter-System Trajectory Design with Manifold Captures

**Yuri Shimane*** **and Koki Ho†**

## ABSTRACT

When traveling across multiple planetary or moon systems, invariant manifold structures may be leveraged to allow for efficient transfer within multi-body dynamics. However, the sole use of these structures is restrictive in many cases, as the manifold may not reach a desired departure or arrival location in the phase space. In particular, the use of low-thrust propulsion together with manifold dynamics requires an optimization framework that captures these mechanisms into a single problem. This work proposes an approach to design gravity-assist low-thrust transfers that leverage manifold structures at departure or arrival. The approach involves a modification to the Sims-Flanagan transcription by incorporating parametrization of arrival to a manifold Poincaré section instead of a celestial body. A key advantage is its use of two-body dynamics for the propagation of the majority of the transfer. This enables large-scale and realistic assessment of possible solutions through a combination of ODE-based propagation of the manifold, and Lagrange coefficients-based propagation of the inter-system portion of the transfer. Leveraging the proposed method, a low-thrust transfer from Earth to the Sun-Venus system, also incorporating an Earth fly-by in between, is studied.

## INTRODUCTION

The interplanetary transport network,[1] which leverages multi-body dynamics for efficient transfers across the solar system, is becoming an increasingly attractive tool for mission designers. For example, in the context of the Earth-Moon system, the Sun-Earth and Earth-Moon manifolds of libration point orbits (LPOs) are often leveraged to construct preliminary designs of low-energy transfers.[2] One possible approach in the cislunar transfer context is to patch two manifolds at some pre-defined Poincaré section (PS), in a fashion similar to the patched-conics method in interplanetary trajectory design. However, this is not possible if the manifolds of the two systems do not intersect in phase space. For instance, a spacecraft leaving the Earth cannot immediately insert into the manifold of a LPO about Venus or Mars, as these do not intersect with the orbit of the Earth.

*PhD Student, School of Aerospace Engineering, Georgia Institute of Technology, Atlanta, GA 30332.
†Assistant Professor, School of Aerospace Engineering, Georgia Institute of Technology, Atlanta, GA 30332.

Accounting for this shortcoming, several previous approaches have been introduced to design conic sections connecting manifold insertion points through a predominantly two-body system in between. The use of manifold structures in interplanetary transfer contexts has been introduced by Topputo et al[3] and Eapen and Sharma.[4] Upon arrival at a PS of a Sun-planet system manifold, Topputo and Belbruno[5] studied the use of weak-stability boundary captures for planetary capture, specifically for the Earth-Mars case. Canales et al[6] leveraged a similar approach for outlining an analytical transfer design method for hopping between planetary moons. All of these works considered impulsive transfers between insertion points from and into manifolds, which may be executed as deep-space maneuvers. This is suitable for considering transfers of spacecraft with high-thrust propulsion, while they fall short of considering transfers of spacecraft with low-thrust propulsion.

Transfers leveraging manifold insertions are of particular interest for low-thrust propulsion, as there is no need for a large braking maneuver at any point. The use of some Sun-planet system LPOs have been studied, and this class of transfers would enable the spacecraft to be brought to these LPOs using low-thrust propulsion alone. For example, the Sun-Mars L1 and L2 halo orbits have been investigated for establishing a permanent communication link between Earth and space systems in the Martian system.[7,8] Shirobokov et al[9] proposed the use of a Sun-Venus L2 halo for placing a space-telescope, permitting earlier detection of potentially hazardous near-earth asteroids (NEAs), while Kovalenko et al[10] considered the use of Sun-Venus L2 LPOs by small spacecraft to enhance the scientific return of the planned Venera-D mission.[11] While beyond the scope of this work, it is also possible to use the LPO as a temporary orbit, transferring further to a final orbit closer to the planet or moon using low-thrust propulsion and leveraging three-body dynamics. Tanaka et al[12] considered the Sun-Mars L1 halos as generating mechanisms for weak-stability boundary captures into the Martian system.

This work presents a low-thrust inter-system trajectory design scheme, where the inter-system portion of the transfer involves a low-thrust phase, rather than impulsive transfers involving large deep-space maneuvers. Furthermore, in the presented framework, leveraging previous transfer design approaches, fly-by's at certain bodies between the departure and arrival may also be incorporated. This enables the preliminary design and solution-space analysis of low-thrust transfers with manifold captures. The inter-system portion is based on the Sims-Flanagan Transcription (SFT),[13,14] which is a direct trajectory optimization approach that approximates the low-thrust acceleration through a discretization. This is particularly suitable for preliminary analysis of transfer opportunities.[15–17] This feature is inherited by the presented method, where exploration of the solution space for inter-system, gravity-assist low thrust transfers with manifold captures can be conducted.

This paper is organized as follows. Firstly, the relevant dynamical models are introduced, along with a discussion on the treatment of the boundaries between the two dynamical regimes. Transformations of the spacecraft state between the two regimes as well as invariant manifold structures within three-body systems are also introduced. Then, the traditional SFT approach, along with the modification made to account for manifold captures is described. Finally,

the proposed method is implemented for a transfer to a Sun-Venus L2 halo orbit, involving an Earth fly-by during its transit.

## DYNAMICAL SYSTEMS MODELING

When considering inter-system trajectories, the majority of the transfer occurs in primarily two-body dynamics, where only the gravitational acceleration of a primary body is relevant. Here, *inter-system* denotes either interplanetary or inter-moon trajectories. For an interplanetary transfer, the spacecraft is mostly under the influence of heliocentric two-body dynamics, while for an inter-moon transfer, it is mostly under the influence of the planet hosting the moons.

In contrast, manifold structures arise specifically when considering three-body dynamics, involving primary and secondary bodies, together with the spacecraft. For an interplanetary transfer, this would correspond to a Sun-planet-spacecraft three-body problem, while for an inter-moon transfer, this would correspond to a planet-moon-spacecraft three-body problem. Figure 1 illustrates a generic scheme of the class of transfers studied in this work.

While one approach in designing inter-system transfers may involve accounting for third-body perturbations throughout the transfer, this is unnecessary in most portions where the perturbing force is minute. There is also a substantive difference in computational resource necessary to compute the trajectories, as purely two-body low-thrust transfers may be effectively approximated by a series of small impulses; the spacecraft state is propagated sequentially using some form of Kepler's equation, introducing velocity discontinuities as $\Delta v$'s along the way. In contrast, the inclusion of the third-body perturbation necessitates the direct integration of equations of motion as ODEs, which is a computationally heavier procedure. The latter in fact enables higher-fidelity modeling of the thrust, where a continuous acceleration due to the thrusters may be incorporated into the ODEs. To benefit from this feature while accounting for the computational time drawback, Yam et al[18] proposed the use of Taylor-integrators in lieu of Runge-Kutta schemes. Nonetheless, ODE-based propagation still remains impractical particularly when large search spaces must be explored at a preliminary mission planning stage. Thus, this work adopts the use of fully two-body inter-system portions, where all perturbing effects are neglected when the spacecraft is located far enough from any celestial body. As a consequence of this choice, the boundary between a fully two-body regime and a three-body regime must be selected with caution.

This section initially describes the propagation schemes available for propagating a low-thrust spacecraft state-vector in the inter-system portion of a transfer. Then, invariant manifolds, which are structures that exist uniquely in the three-body system, are introduced. This is followed by a treatment of the boundary between the two-body and three-body systems. Finally, the coordinate transformation applied at the boundary is introduced.

### Trajectory Propagation in the Inter-System Portion

In the inter-system portion, the motion of the spacecraft may be assumed to be void of any perturbing forces besides the gravity of the central body and its own thruster. Then, the continuous, low-thrust acceleration may be further

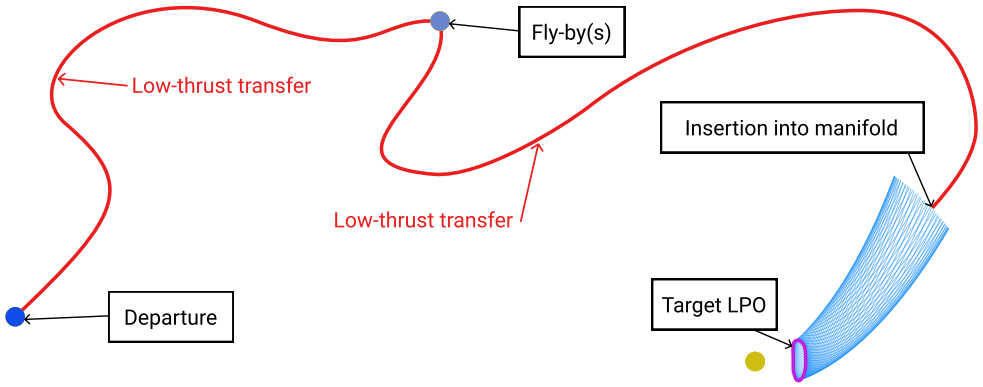


**Figure 1. Concept of interplanetary low-thrust trajectory with manifold capture**

approximated by a series of impulsive $\Delta v$'s. This results in the spacecraft motion being described by Keplerian dynamics, and the two-body state-vector of a spacecraft may be propagated forward in time using Lagrange coefficients $\mathrm{f}$ and $\mathrm{g}$ by

$$\boldsymbol{r} = \mathrm{f}\boldsymbol{r}_0 + \mathrm{g}\boldsymbol{v}_0 \tag{1}$$

$$\boldsymbol{v} = \dot{\mathrm{f}}\boldsymbol{r}_0 + \dot{\mathrm{g}}\boldsymbol{v}_0 \tag{2}$$

where $\boldsymbol{r}$ is the position vector and $\boldsymbol{v}$ is the velocity vector. For the use of $\mathrm{f}$, $\mathrm{g}$, and their derivatives, see Bate et al.[19] In this way, a low-thrust trajectory may be discretized into $n$ segments, each containing a single impulsive change in velocity. The impulsive $\Delta v$ added at each segment, denoted as $\Delta \boldsymbol{v}_k$, is to be passed as a decision variable to an optimizer, and its treatment is discussed in the next Section. It is also noted that in this way, the spacecraft mass is updated discontinuously at each impulse via the relation

$$m_{k+1} = m_k - \Delta m_k \tag{3}$$

where $\Delta m_k$ corresponds to the propellant consumed within the $k^{\mathrm{th}}$ segment, given by

$$\Delta m_k = \Delta t_{\text{segment}} \tau_k \dot{m} \tag{4}$$

where $\Delta t_{\text{segment}}$ is the duration of a segment, $\tau_k$ is the throttle of the thruster between $0$ and $1$ used during the $k^{\mathrm{th}}$ segment, and $\dot{m}$ is the mass-flow rate of the thruster. The Algorithm for propagating the trajectory through this approach is presented in the Appendix.

**Three-Body System, Libration Point Orbits, and Manifolds**

The three-body problem, first introduced by Sir Isaac Newton in 1687, is a system with no closed-form analytical solution. Due to its complexity, this problem is commonly studied in approximate models, which are known to yield insightful preliminary solutions that may be extended successfully to the full ephemeris model. A common approximation involves the circular restricted three-body problem (CR3BP), where the motion of the two bodies are considered to be circular about their barycenter, and the mass of the spacecraft is considered to be negligible compared to the mass of the two celestial bodies. The CR3BP is commonly studied in a rotating frame, where the x-axis connects the two celestial bodies, the z-axis points to the direction of the angular momentum vector of these two bodies, and the y-axis completes the triad. The equations of motion of the CR3BP are given by

$$\begin{aligned} \ddot{x} - 2\dot{y} &= \frac{\partial U}{\partial x} \\ \ddot{y} + 2\dot{x} &= \frac{\partial U}{\partial y} \\ \ddot{z} &= \frac{\partial U}{\partial z} \end{aligned} \tag{5}$$

where $U$ is the pseudo-potential given by

$$U = \frac{x^2 + y^2}{2} + \frac{1-\mu}{r_1} + \frac{\mu}{r_2} \tag{6}$$

and $\mu$ is the mass-parameter of the CR3BP system, given by

$$\mu = \frac{M_2}{M_1 + M_2} \tag{7}$$

where $M_1$ is the mass of the primary body, and $M_2$ is the mass of the secondary body.

*Libration Point Orbits* While motions in the three-body system are chaotic, there are five well-known equilibrium points, known as libration or Lagrange points, along with periodic orbits in the vicinity of these points. Of particular interest in this work are periodic orbits around the L1 and L2 points, also referred to as LPOs, due to their relatively close proximity to a body of interest, hence enabling their use as either a science orbit or a transition orbit. In this work, the halo orbit family is considered as target LPOs, due to their saddle-stable property that leads to the existence of invariant manifolds, and their spatial structure compared to the likes of Lyapunov orbits. The latter property is suitable for mission design, as spatial motions enable the possibility for observing or accessing surfaces of the body outside of its equatorial plane.

To construct a LPO, a typical strategy involves constructing an initial guess in simplified systems, followed by a numerical correction scheme such as shooting methods or collocation. In this work, the initial guess halo orbit

is constructed via a third-order approximation of the periodic motion,[20] followed by a single-shooting correction leveraging the xz-plane symmetry of the halo orbit family.[21]

*Manifolds* Given a state-vector $\boldsymbol{y}_0$ along the LPO, its invariant manifolds may be obtained by perturbing states on the LPO along the local stable or unstable eigenvector direction. Starting with $\boldsymbol{y}_0$ and LPO period $P$, the state-transition matrix $\Phi$ is obtained from the initial value problem

$$\begin{aligned} \dot{\Phi} &= A\Phi \\ \Phi(0) &= \mathbf{I}_{6,6} \end{aligned} \tag{8}$$

where the $A$ matrix is given by

$$A(\boldsymbol{y}) = \left[\begin{array}{c|c} \mathbf{0}_{3,3} & \mathbf{I}_{3,3} \\ \hline U_{\boldsymbol{yy}} & 2\boldsymbol{\Omega} \end{array}\right] \;,\; \boldsymbol{\Omega} = \begin{bmatrix} 0 & 1 & 0 \\ -1 & 0 & 0 \\ 0 & 0 & 0 \end{bmatrix} \tag{9}$$

where $U_{\boldsymbol{yy}}$ is a 3-by-3 matrix consisting of second order partial derivatives of $U$, from equation (6). The stable and unstable eigenvectors of the problem, $\mathbf{Y}^s$ and $\mathbf{Y}^u$, are obtained from solving the eigenvalue problem for the monodromy matrix $\Phi(P)$. Then, the initial conditions of the stable and unstable manifold branches are obtained by perturbing the state along the LPO in the eigenvector direction with some magnitude $\epsilon$.

$$\boldsymbol{y}^s_{ptb}(t_{\text{LPO}}) = \boldsymbol{y}_0(t_{\text{LPO}}) \pm \epsilon \mathbf{Y}^s(t_{\text{LPO}}) \tag{10}$$

$$\boldsymbol{y}^u_{ptb}(t_{\text{LPO}}) = \boldsymbol{y}_0(t_{\text{LPO}}) \pm \epsilon \mathbf{Y}^u(t_{\text{LPO}}) \tag{11}$$

where $t_{\text{LPO}}$ denotes the time along the LPO, and $0 \leq t_{\text{LPO}} \leq P$. The stable branches are obtained by propagating the initial state $\boldsymbol{y}^s_{ptb}(t_{\text{LPO}})$ for some time $\Delta t_{\text{manifold}} < 0$, while the unstable branches are obtained by propagating the initial state $\boldsymbol{y}^u_{ptb}(t_{\text{LPO}})$ for some time $\Delta t_{\text{manifold}} > 0$. Figure 2 shows an example of stable and unstable manifolds for a Sun-Venus L2 halo orbit. In addition, utilizing the corresponding stable and unstable eigenvalues, the stability index $\nu$ of the LPO may be computed by

$$\nu = \frac{1}{2}|\lambda^s + \lambda^u| \tag{12}$$

**Approximate Boundary Between Two-body and Three-Body Regimes**

Traditionally, preliminary inter-system trajectory designs leverage patched-conics approximations, where the primary gravitational body is instantaneously switched between the Sun and a planet, in the case of an interplanetary transfer, or between the planet and a moon, in the case of an inter-moon transfer, at the sphere of influence (SOI),

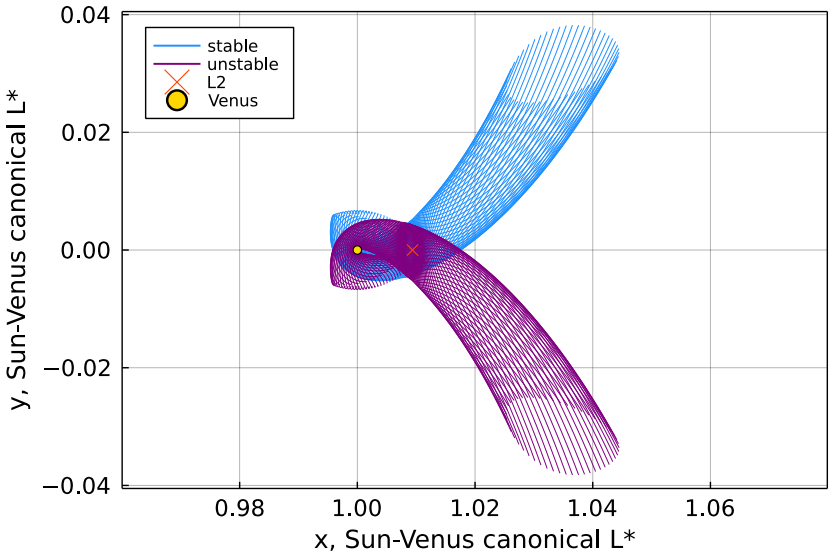


**Figure 2. Sun-Venus L2-halo orbit, unstable, and stable manifold, in Sun-Venus rotating frame, centered at Venus**

defined as

$$r_{\text{SOI}} = a_{M_2}\left(\frac{M_2}{M_1}\right)^{2/5} \tag{13}$$

where $a_{M_2}$ is the semi-major axis of the smaller body. While the SOI is a useful tool for designing transfers with hyperbolic departure or arrival, it is unsuitable to be used for switching dynamics between two-body and three-body regimes; in fact, LPOs commonly exist close to the SOI.

As such, an alternative radius must be defined to construct a PS of a manifold, where the switch between the two-body and three-body dynamics may be done without significant deviation on the trajectory beyond this point. This is done by adopting the approach previously introduced by Canales et al,[6] where a threshold on the ratio of the accelerations is defined as

$$\gamma = \frac{\|\boldsymbol{a}_2\|}{\|\boldsymbol{a}_1\|} \tag{14}$$

where $\boldsymbol{a}_1$ and $\boldsymbol{a}_2$ are accelerations due to the primary and secondary bodies, respectively. Figure 3 shows the variation of $\gamma$ as a function of Venus radii along the x-axis from Venus.

Consider the location where $\gamma = 10^{-3}$ as a threshold radius; it is at approximately 1,000 times Venus radii, and well beyond the SOI. The value of $\gamma$ is a configurable parameter, whereby a mission designer may choose an appropriate value based on the desired fidelity of the preliminary trajectory or some mission requirements. Figure 4 shows the deviation of the states, propagating backward in time from the PS where $\gamma = 10^{-3}$ using the two-body equations of motion

$$\ddot{\boldsymbol{r}} = -\frac{GM_1}{r^3}\boldsymbol{r} \tag{15}$$

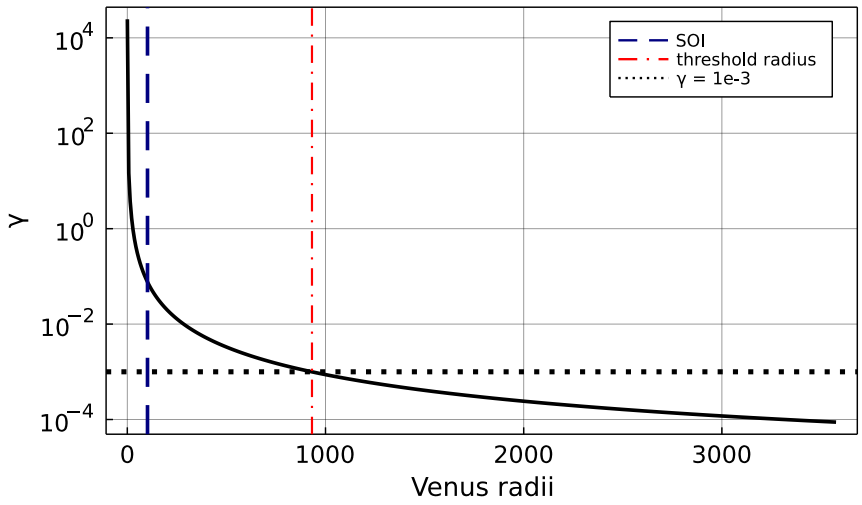


**Figure 3. Acceleration ratio in the vicinity of Venus, along Sun-Venus x-axis**

and the CR3BP equations of motion (5). The position offsets are within 2%, and the velocity offsets are within about 5% with respect to the length and velocity scale of the Sun-Venus system. This is deemed to be small enough for preliminary design, as these offsets may be corrected further when transitioning the solution to higher fidelity models.

### Coordinate Frames and Transformations

The heliocentric phase of the transfer is designed in the ecliptic reference frame centered at the Sun, specifically the ECLIPJ2000 frame following JPL's SPICE conventions. In contrast, the approach phase of the transfer is modeled in the CR3BP frame, which is a rotating frame with the x-axis fixed to the Sun-planet line, and the z-axis parallel to the axis of rotation of the planet's orbit. In this frame, the planet's motion around the Sun is assumed to be circular.

Given the planet's Keplerian orbital elements, transforming a state-vector defined in the CR3BP frame to the ECLIPJ2000 consists of a series of transformations. The first transformation $\boldsymbol{T}_1$ takes the CR3BP state and converts it into an inertial, intermediate state, using the argument of periapsis ($\omega$) and true anomaly ($f$). The corresponding transformation matrix is given by

$$\boldsymbol{T}_1(t) = \begin{bmatrix} \cos \upsilon_1(t) & -\sin \upsilon_1(t) & 0 & 0 & 0 & 0 \\ \sin \upsilon_1(t) & \cos \upsilon_1(t) & 0 & 0 & 0 & 0 \\ 0 & 0 & 1 & 0 & 0 & 0 \\ -\omega_{\text{CR3BP}} \sin \upsilon_1(t) & -\omega_{\text{CR3BP}} \cos \upsilon_1(t) & 0 & \cos \upsilon_1(t) & -\sin \upsilon_1(t) & 0 \\ \omega_{\text{CR3BP}} \cos \upsilon_1(t) & -\omega_{\text{CR3BP}} \sin \upsilon_1(t) & 0 & \sin \upsilon_1(t) & -\cos \upsilon_1(t) & 0 \\ 0 & 0 & 0 & 0 & 0 & 1 \end{bmatrix} \tag{16}$$

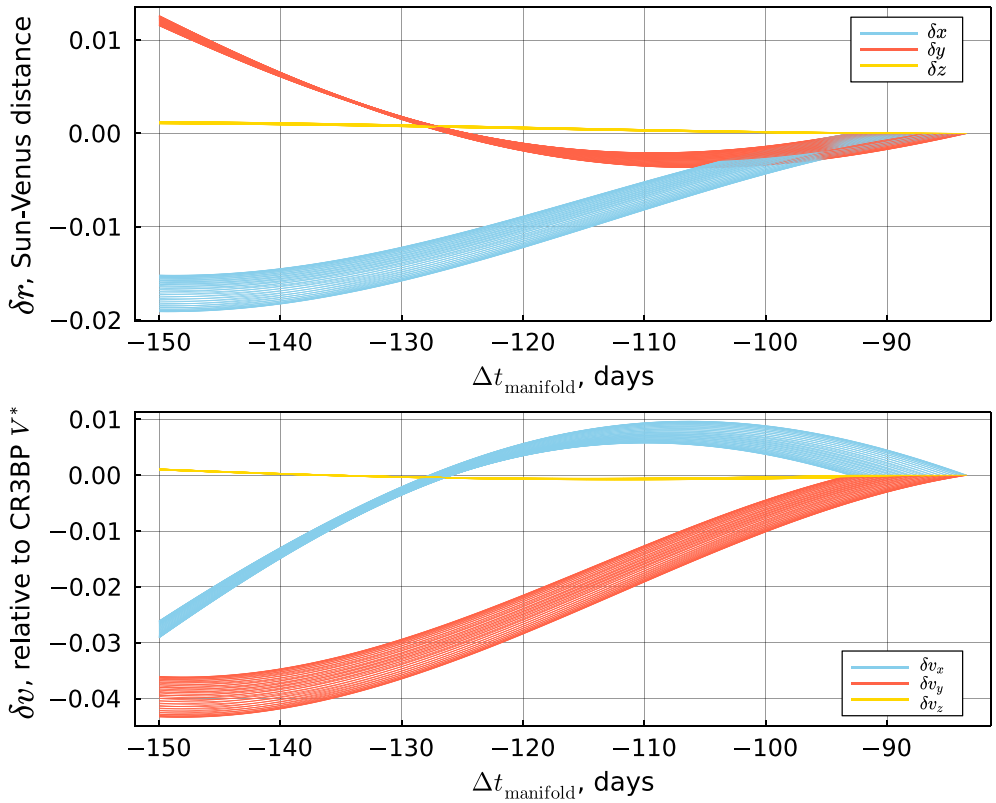


**Figure 4. Deviation of states in two-body against CR3BP regimes, propagated from $\Gamma$ where $\gamma = 10^{-3}$**

where $\omega_{\text{CR3BP}}$ is the rotational rate of the Sun-planet system, and the rotation angle $\upsilon_1(t)$ is given by $\upsilon_1(t) = \omega + f(t)$, where $f$ has an epoch-dependency. Then, a clockwise rotation $\boldsymbol{T}_2$ about the x-axis by the inclination $(i)$ and a final clockwise rotation $\boldsymbol{T}_3$ about the z-axis by the right-ascension of ascending node $(\Omega)$ of the position and velocity vectors are applied independently.

$$\boldsymbol{T}_2(i) = \begin{bmatrix} \boldsymbol{t}_2(i) & 0_{3\times3} \\ 0_{3\times3} & \boldsymbol{t}_2(i) \end{bmatrix}, \ \boldsymbol{t}_2(i) = \begin{bmatrix} 1 & 0 & 0 \\ 0 & \cos i & -\sin i \\ 0 & \sin i & \cos i \end{bmatrix} \tag{17}$$

$$\boldsymbol{T}_3(\Omega) = \begin{bmatrix} \boldsymbol{t}_3(\Omega) & 0_{3\times3} \\ 0_{3\times3} & \boldsymbol{t}_3(\Omega) \end{bmatrix}, \ \boldsymbol{t}_3(\Omega) = \begin{bmatrix} \cos\Omega & -\sin\Omega & 0 \\ \sin\Omega & \cos\Omega & 0 \\ 0 & 0 & 1 \end{bmatrix} \tag{18}$$

The combined transformation from CR3BP to ECLIPJ2000, $\boldsymbol{T}_{\text{EC}}(t)$, is given by

$$\boldsymbol{T}_{\text{EC}}(t) = \boldsymbol{T}_3\boldsymbol{T}_2\boldsymbol{T}_1(t) \tag{19}$$

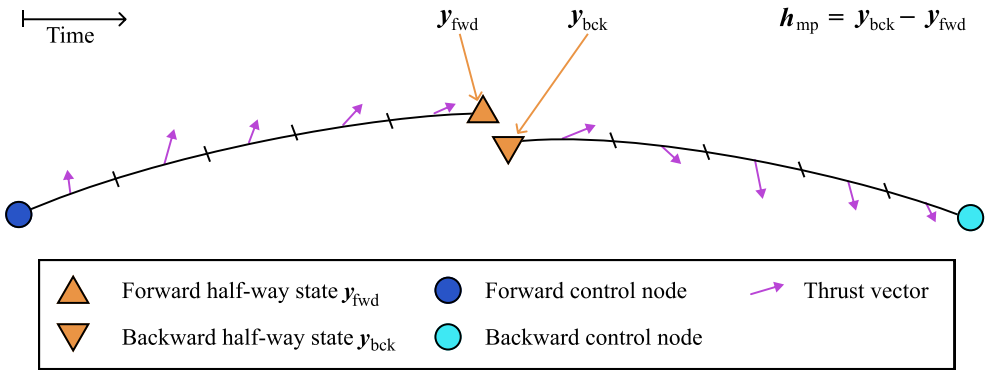


**Figure 5. Leg with low-thrust discretization in Sims-Flanagan Transcription, adapted from Shimane and Ho[22]**

Note that the semi-major axis and eccentricity of the planet's orbit are not used in the sequence of transformation since the planet's orbit is assumed to be circular in the CR3BP.

## OPTIMIZATION PROBLEM SETUP

The manifold-capture segment is incorporated into the interplanetary trajectory design problem by modifying the transcription of the arrival parameters from a traditional SFT.

### Sims-Flanagan Transcription

The SFT considers an interplanetary trajectory in terms of $N$ *legs*, connecting two consecutive planetary bodies visited by the spacecraft. At each planetary visit, a *control-node* is defined based on the ephemeris of the planet at a given epoch and an associated $v_\infty$ vector. In the case of a fly-by control-node, two $v_\infty$ vectors are defined for the in-coming and out-going legs, respectively. Over each leg, the control-nodes at both ends are propagated forward and backward in time for half of the flight time of the leg, and the half-way point of each leg is denoted as the *match-point*. The optimizer must drive the residual between the forward and backward propagated states at the match-point to $0$ by tuning the control-nodes along with the thrust controls. For the propagation, each leg is discretized into $n$ equal-time *segments*, and the thrust control is kept constant over each segment. The original formulation involves further simplifying the propagation by considering Keplerian arcs with an impulsive $\Delta$V at the center of each segment to approximate the low-thrust maneuver,[13] an approach that has been implemented in multiple tools such as MALTO[14] and GALLOP.[15] Figure 5 illustrates a single leg of a trajectory, with $n = 10$ segments.

The trajectory is propagated using equations (1) and (2), using previously developed efficient implementations.[23,24] The impulsive $\Delta\boldsymbol{v}$ applied at the half-way point of each segment is given by

$$\Delta\boldsymbol{v} = \frac{T_{\max}}{m}\Delta t_{\text{seg}}\tau\boldsymbol{T}_{\text{EL}}(\boldsymbol{r},\boldsymbol{v})\left[\cos(\theta)\cos(\beta),\sin(\theta)\cos(\beta),\sin(\beta)\right]^{\text{T}} \tag{20}$$

where $T_{\max}$ is the maximum achievable thrust, $m$ is the current mass of the spacecraft, $\Delta t_{\text{seg}} = \dfrac{t_{\text{leg}}}{n}$ is the duration of

each segment, $\tau$ is the throttle value between 0 and 1, and $\theta$ and $\beta$ are the respective in-plane and out-of-plane angles. The angles are defined in the local vertical, local horizon (LVLH) frame, where $\theta = 0$ along the velocity vector with $\theta > 0$ clockwise, and $\beta = 0$ on the local horizontal plane with $\beta > 0$ on the local normal direction. The 3 by 3 matrix $\boldsymbol{T}_{\mathrm{EL}}(\boldsymbol{r}, \boldsymbol{v})$ transforms the vector into the inertial frame. The parameters $\tau$, $\theta$, and $\beta$ for each segment along each phase are part of the decision vector, as will be described in the next section. The mass of the spacecraft is also updated at the half-way point of each segment using expressions (3) and (4).

*Problem Formulation and Decision Vector* The trajectory optimization problem may be formulated to maximize the final mass

$$\begin{aligned} \min_{\boldsymbol{x}} \quad & -m_f \\ \text{such that} \quad & \boldsymbol{h}_{\text{mp}} = 0 \\ & g_{\mathrm{TOF}} \leq 0 \\ & \boldsymbol{g}_{\text{fly-by}} \leq 0 \end{aligned} \tag{21}$$

where $\boldsymbol{h}_{\text{mp}}$ is a set of equality constraints to ensure continuity at the match-points, $g_{\mathrm{TOF}}$ is an inequality constraint on the total time of flight, and $\boldsymbol{g}_{\text{fly-by}}$ is an inequality constraint for any fly-by the spacecraft undergoes. These will be discussed further following the description of the decision vector $\boldsymbol{x}$, given by

$$\boldsymbol{x} = [\boldsymbol{c}_{\text{launch}},\, \boldsymbol{c}^1_{\text{fly-by}},\, \ldots,\, \boldsymbol{c}^{N-1}_{\text{fly-by}},\, \boldsymbol{c}_{\text{arrival}},\, \boldsymbol{\tau}^1,\, \ldots,\, \boldsymbol{\tau}^N] \tag{22}$$

where $\boldsymbol{c}$ are parameters at the initial, intermediate, and final nodes along the transfer, and $\boldsymbol{\tau}$ are the discretized controls of the thruster for each leg between $i = 1, \ldots, N$. For any mission, the launch parameter $\boldsymbol{c}_{\text{launch}}$ is given by

$$\boldsymbol{c}_{\text{launch}} = [t_0, m_0, v^1_\infty, \alpha^1, \delta^1] \tag{23}$$

representing, in order, the launch epoch $t_0$, initial mass $m_0$, $v_\infty$ magnitude, right-ascension $\alpha$, and declination $\delta$ at launch. The two angles $\alpha$ and $\delta$ are defined with respect to the LVLH frame of the planet's motion, and the position and velocity of the spacecraft is constructed via

$$\begin{bmatrix} \boldsymbol{r} \\ \boldsymbol{v} \end{bmatrix} = \begin{bmatrix} \boldsymbol{r}_{\text{planet}} \\ \boldsymbol{v}_{\text{planet}} \end{bmatrix} + \begin{bmatrix} \boldsymbol{0} \\ \boldsymbol{v}_\infty \end{bmatrix} \tag{24}$$

where $\boldsymbol{r}_{\text{planet}}$ and $\boldsymbol{v}_{\text{planet}}$ are the position and velocity vectors of the planet at epoch $t_0$, and $\boldsymbol{v}_\infty$ is a vector constructed with

$$\boldsymbol{v}_\infty = v_\infty \boldsymbol{T}_{\mathrm{EL}}(\boldsymbol{r}_{\text{planet}}, \boldsymbol{v}_{\text{planet}})\, [\cos(\alpha)\cos(\delta), \sin(\alpha)\cos(\delta), \sin(\delta)]^{\mathrm{T}} \tag{25}$$

If the transfer has gravity assist(s) along its way, there will also be one or more fly-by parameters $\boldsymbol{c}_{\text{fly-by}}$, given by

$$\boldsymbol{c}^j_{\text{fly-by}} = [\Delta t^j, m^{j+1}, v_\infty^{j+1}, \alpha_-^{j+1}, \delta_-^{j+1}, \alpha_+^{j+1}, \delta_+^{j+1}], \;\; j \in [1, N-1] \tag{26}$$

where the superscript $j$ represents the $j^{\text{th}}$ visited body by the spacecraft after launch. In this case, the epoch variable from $\boldsymbol{c}_{\text{launch}}$ is replaced by the time-of-flight since the last visited node, denoted as $\Delta t^j$. There are also pairs of right-ascension and declination, $\alpha_{+/-}^{j+1}$ and $\delta_{+/-}^{j+1}$, corresponding to the in-coming and out-going values. If powered fly-by's are also to be considered, there should also be a pair of $v_{\infty,+/-}^{j+1}$ values. Finally, the arrival parameters $\boldsymbol{c}_{\text{arrival}}$ are given by

$$\boldsymbol{c}_{\text{arrival}} = [\Delta t^N, m^{N+1}, v_\infty^{N+1}, \alpha^{N+1}, \delta^{N+1}] \tag{27}$$

which consists of the same components as the launch parameters except for the epoch, which is again replaced by the time-of-flight since the last visited node. Note that the final mass $m_f$, which is the objective of the problem, is directly obtained from the arrival node, since $m^{N+1} = m_f$.

The thrust control vector $\boldsymbol{\tau}^i$ represents the sequence of controls the thruster must undertake during the $i^{\text{th}}$ leg. It is given by

$$\boldsymbol{\tau}^i = [\tau_1^i,\, \theta_1^i,\, \beta_1^i,\, \ldots,\, \tau_k^i,\, \theta_k^i,\, \beta_k^i,\, \ldots,\, \tau_n^i,\, \theta_n^i,\, \beta_n^i], \;\; i \in [1, N] \;, k \in [1, n] \tag{28}$$

where $\tau$, $\theta$, and $\beta$ are as defined for equation (20).

*Bounds on the Decision Vector* Each component of the decision vector is bounded by lower and upper bounds. The launch epoch $t_0$ is bounded by the desirable launch window for a mission. The masses $m$ are bounded between 0 and 1 when non-dimensionalizing the problem using the initial mass. The times of flight between two consecutive bodies are bounded by considering the orbital periods of the planets at the forward and backward control-nodes, as listed by Englander and Englander[25] for the Evolutionary Mission Trajectory Generator (EMTG)[26]; considering the orbital periods $P_{\text{fwd}}$ and $P_{\text{bck}}$ and semi-major axes $a_{\text{fwd}}$ and $a_{\text{bck}}$ of the forward and backward planets, the lower-bound is given by

$$\Delta t_{\text{lb}} = \begin{cases} \dfrac{P_{\text{fwd}}}{2} \text{, if leg between same planet} \\ 0.1 \min(P_{\text{fwd}}, P_{\text{bck}}) \text{, otherwise} \end{cases} \tag{29}$$

**Table 1. Variable bounds of Sims-Flanagan Transcription Problem**

| Variable type | Lower bound | Upper bound |
|---|---|---|
| Epoch, $t_0$ | Earliest launch date | Latest launch date |
| Time of flight per leg | $\Delta t_{lb}$ | $\Delta t_{ub}$ |
| Mass | 0 | 1 |
| V-infinity | 0 | $v_{\infty,\max}$ |
| $\alpha$ | $-\pi$ | $\pi$ |
| $\delta$ | $-\pi$ | $\pi$ |
| $\tau$ | 0 | 1 |
| $\theta$ | $-\pi$ | $\pi$ |
| $\beta$ | $-\pi/2$ | $\pi/2$ |

and the upper-bound is given by

$$\Delta t_{\text{ub}} = \begin{cases} 5P_{\text{fwd}}\,, \text{if leg between same planet} \\ 2\max(P_{\text{fwd}}, P_{\text{bck}})\,, \text{ if } \max(a_{\text{fwd}}, a_{\text{bck}}) < 2\text{AU} \\ \max(P_{\text{fwd}}, P_{\text{bck}})\,, \text{ if } \max(a_{\text{fwd}}, a_{\text{bck}}) \geq 2\text{AU} \end{cases} \tag{30}$$

The throttle $\tau$ is bounded between 0 and 1, while the angles $\theta$ and $\beta$ are bounded from $-\pi$ to $\pi$ and from $-\pi/2$ to $\pi/2$, respectively. The $v_\infty$ magnitude is bounded between 0 and a multiple of the parabolic excess velocity in the heliocentric frame at a distance $\max(a_{\text{fwd}}, a_{\text{bck}})$ from the Sun. The two $v_\infty$ angles $\alpha$ and $\delta$ are also bounded between $-\pi$ and $\pi$. Table 1 summarizes the bounds on the variables for the SFT problem.

*Problem Constraints* The constraints of this problem consists of the match-point constraint(s), $\boldsymbol{h}_{mp}$, time of flight constraint, $g_{\text{TOF}}$, and fly-by altitude constraint(s), $\boldsymbol{g}_{\text{fly-by}}$. The match-point constraint is an equality constraint that consists of the residuals from the forward and backward propagation of the control-nodes; this is computed for each leg of the transfer and is given by

$$\boldsymbol{h}^i_{mp} = \boldsymbol{y}_{\text{bck}} - \boldsymbol{y}_{\text{fwd}} = 0\,, \;\; i \in [1, N] \tag{31}$$

where $\boldsymbol{y}_{\text{fwd}}$ and $\boldsymbol{y}_{\text{bck}}$ are the forward and backward propagation of the position, velocity, and mass. The time-of-flight constraint is an inequality constraint to ensure the spacecraft arrives at its intended destination within a predefined duration, $\text{TOF}_{\text{max}}$. It is given by the summation of the times of flight for each segment

$$g_{\text{TOF}} = \text{TOF} - \text{TOF}_{\text{max}} = \sum_{i=1}^{N} \Delta t^i - \text{TOF}_{\text{max}} \leq 0 \tag{32}$$

The fly-by altitude constraint is also an inequality constraint that ensures a minimum safety altitude, $h_{\text{safe}}$, when a spacecraft conducts a gravity-assist. For each gravity-assist, this constraint is defined as

$$\boldsymbol{g}_{\text{fly-by}} = (r_{\text{planet}} + h_{\text{safe}}) - \frac{\mu_{\text{planet}}}{v_\infty^2}\left[1/\sin\left(\frac{\delta_{\text{turn-angle}}}{2}\right) - 1\right] \leq 0 \tag{33}$$

where $\delta_{\text{turn-angle}}$ is the turn-angle around the planet

$$\delta_{\text{turn-angle}} = \arccos\left(\frac{\boldsymbol{v}_\infty^- \cdot \boldsymbol{v}_\infty^+}{v_\infty^- v_\infty^+}\right) = \arccos\left(\frac{\boldsymbol{v}_\infty^- \cdot \boldsymbol{v}_\infty^+}{v_\infty^2}\right) \tag{34}$$

The denominator may be simplified if the fly-by is not powered, since the incoming and outgoing $v_\infty$ vectors must have equal magnitudes. This is computed at each fly-by control-node, $\boldsymbol{c}^j_{\text{fly-by}}$.

**Modifications to Arrival Parameters for Targeting Libration Point Orbits**

To incorporate ballistic arrivals into manifolds, the arrival parameters (27) must be replaced by one that approximates the spacecraft's state in a three-body regime. To this end, the stable manifold of the LPO is utilized; instead of starting the final backward segment of the trajectory from the ephemeris of the planet, the control-node is set on a state-vector lying on a PS that is a cross-section of the manifold. This ensures the spacecraft to insert into the LPO through a ballistic path along the manifold. Since the control-node no longer represents an arrival to a planetary body, such arrival control node does not have an associated $v_\infty$ value. It is noted that the chosen LPO must have a sufficiently low Jacobi constant such that the stable manifold extends outside the SOI.

Two approaches to formulate such PS-based arrival parameters are considered; the first involves pre-defining a specific PS in the CR3BP frame, while the second involves letting the optimizer choose a PS based on lower and upper bounds on the time spent on the manifold between the PS and the LPO. The former is denoted as the fixed-PS arrival, while the latter is denoted as the free-PS arrival.

*Targeting Libration Point Orbit at Fixed Poincaré Section* In the fixed-PS arrival case, the PS is located at a fixed travel time $\Delta t_{\text{manifold}}$ away along the manifold from the targeted LPO. Such PS may be parameterized by an angle parameter $\phi \in [0, 1]$, which may be understood as the location around the LPO to which a manifold branch is connected, given by

$$\phi = \frac{t_{\text{LPO}}}{P} \tag{35}$$

where $P$ is the period of the LPO, and $t_{\text{LPO}} \in [0, P]$ is the propagation time along the LPO from an initial condition on the xz-plane in the CR3BP. Then, the cross-section of the manifold may be parameterized as a curve $\Gamma$, which takes in $\phi$ and returns the corresponding position and velocity $\boldsymbol{y}^{\text{CR3BP}}$ on the PS. The arrival parameters from expression (27)

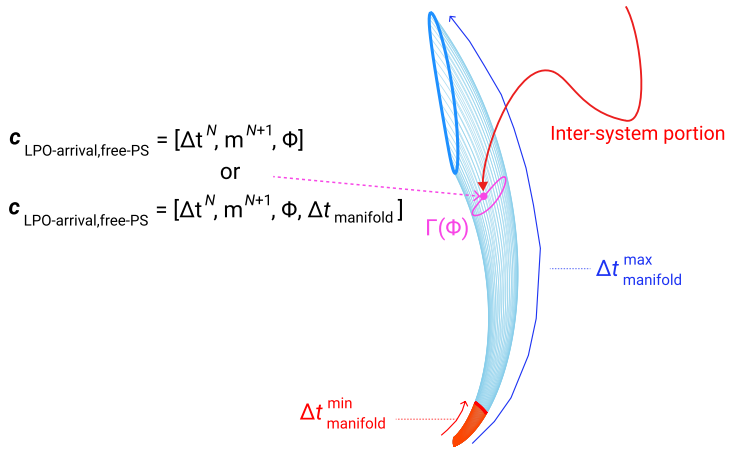


**Figure 6. Representation of arrival condition at $\Gamma$ along the stable manifold**

is replaced by

$$\boldsymbol{c}_{\text{LPO-arrival, fixed-PS}} = \left[\Delta t^N, m^{N+1}, \phi\right] \tag{36}$$

where the terms $\Delta t^N$ and $m^{N+1}$ remain the same as for the nominal case. These parameters are illustrated in Figure 6. Given these arrival parameters, the control-node is computed by Algorithm 1.

**Algorithm 1** Evaluation of control-node for fixed-PS arrival

**Require:** $\Gamma$, $\boldsymbol{c}_{\text{LPO-arrival, fixed-PS}} = \left[\Delta t^N, m^{N+1}, \phi\right]$

$\boldsymbol{y}^{\text{CR3BP}}_{\text{LPO-arrival, fixed-PS}} = \Gamma(\Phi)$ ▷ obtain control-node state-vector on PS in CR3BP

$\boldsymbol{y}^{\text{ECLIPJ2000}}_{\text{LPO-arrival, fixed-PS}} = \boldsymbol{T}_{\text{EC}}(t^N)\boldsymbol{y}^{\text{CR3BP}}_{\text{LPO-arrival, fixed-PS}}$ ▷ transform from CR3BP to ECLIPJ2000 with equation (19)

*Targeting Libration Point Orbit at Free Poincaré Section* In the free-PS arrival case, an additional parameter is required to first construct the PS that cuts through a manifold. Then, similarly to the previous case, a curve $\Gamma$ is used to uniquely locate the position and velocity from the angle parameter $\phi$. In this case, the arrival parameters are given by

$$\boldsymbol{c}_{\text{LPO-arrival, free-PS}} = \left[\Delta t^N, m^{N+1}, \phi, \Delta t_{\text{manifold}}\right] \tag{37}$$

where $\Delta t_{\text{manifold}}$ is the time spent in the capture segment of the manifold. Again, these parameters are illustrated in Figure 6. Note that for a capture segment, a stable manifold is used, making $\Delta t_{\text{manifold}}$ a negative value. Also, the time of flight constraint from expression (32) must be modified to also include $\Delta t_{\text{manifold}}$, and becomes

$$g_{\text{TOF}} = \text{TOF} + |\Delta t_{\text{manifold}}| - \text{TOF}_{\text{max}} = \sum_{i=1}^{N} \Delta t^i + |\Delta t_{\text{manifold}}| - \text{TOF}_{\text{max}} \leq 0 \tag{38}$$

The value of $\Delta t_{\text{manifold}}$ is bounded between the shortest time spent on the manifold $\Delta t^{\text{min}}_{\text{manifold}}$ such that the spacecraft reaches a point where $\gamma = 10^{-3}$, and a user-defined longest time spent on the manifold $\Delta t^{\text{max}}_{\text{manifold}}$. Given the arrival

**Table 2. Sun-Venus CR3BP system parameters**

| $\mu$ | $L^*$, km | $T^*$, s |
|---|---|---|
| 2.44783230e-06 | 1.08209525e+08 | 3.08988197e+06 |

**Table 3. Sun-Venus L2 halo orbit parameters**

| Period | $x_0$ | $y_0$ | $z_0$ | $v_{x0}$ | $v_{y_0}$ | $v_{z0}$ | Stability index $\nu$ |
|---|---|---|---|---|---|---|---|
| 3.09829484 | 1.00764168 | 0. | 1.25284860e-03 | 0. | 9.73267997e-03 | 0. | 785.6969 |

parameters from $\boldsymbol{c}_{\text{LPO-arrival, free-PS}}$, the control-node is computed by Algorithm 2.

**Algorithm 2** Evaluation of control-node for free-PS arrival

**Require:** $\boldsymbol{y}^s_{ptb}$, $\boldsymbol{c}_{\text{LPO-arrival, free-PS}} = \left[\Delta t^N, m^{N+1}, \phi, \Delta t_{\text{manifold}}\right]$

$\Gamma \leftarrow \texttt{propagate}(\boldsymbol{y}^s_{ptb}, t = \Delta t_{\text{manifold}})$ ▷ Propagate manifold by $\Delta t_{\text{manifold}}$

$\boldsymbol{y}^{\text{CR3BP}}_{\text{LPO-arrival, fixed-PS}} = \Gamma(\Phi)$ ▷ obtain control-node state-vector on PS in CR3BP

$\boldsymbol{y}^{\text{ECLIPJ2000}}_{\text{LPO-arrival, fixed-PS}} = \boldsymbol{T}_{\text{EC}}(t^N)\boldsymbol{y}^{\text{CR3BP}}_{\text{LPO-arrival, fixed-PS}}$ ▷ transform from CR3BP to ECLIPJ2000 with equation (19)

### Optimization Method

The evaluation of the objective of a SFT problem is trivial since the final mass $m^N$ is part of the decision vector. In contrast, the evaluation of the constraints is more involved, and as such the difficulty of the problem arises in obtaining feasible solutions. Furthermore, the design space typically consists of multiple local optima. To tackle these challenges, a common approach consists of wrapping a local gradient-based search method with a monotonic basin hopping pseudo-algorithm (MBH) for global exploration of the trade space, where gradient-based methods such as SNOPT[27] and IPOPT[28] can successfully drive the decision vector to a feasible solution. MBH has been initially introduced by Wales and Doye[29] for optimizing a problem with a funnel structure, and has since been found to be particularly effective by multiple authors for interplanetary trajectory design problems.[17,25,30,31]

## OPTIMIZATION RESULTS

As an example, a low-thrust transfer from Earth to Venus with an Earth fly-by, inserting into a Venus-L2 halo orbit of out-of-plane amplitude 150,000 $\mathrm{km}$ is considered. A launch window between May 1st, 2022 and May 1st, 2024, with a total time of flight within 3 years is considered. The maximum launch $v_\infty$ is set to $1.5\,\mathrm{km/s}$. The thruster is set to have a constant Isp of $3500\,\mathrm{s}$ and constant maximum thrust of $0.4\,\mathrm{N}$, with a spacecraft wet mass of $4100\,\mathrm{kg}$. These parameters are chosen by taking the BepiColombo mission, headed to Mercury, as reference. The SFT problem is constructed using $n = 20$ segments in each leg. The Sun-Venus CR3BP system parameters and the targeted L2 halo orbit, are given in Table 2 and 3 respectively. The period, position, and velocity in Table 3 are in canonical scales of the CR3BP system. Ephemerides are taken from JPL's de440 bsp file. Figure 7 shows the stable manifold of the corresponding LPO, along with $\Gamma$ located at $\Delta t_{\text{manifold}}$ corresponding to $-90$, $-120$, and $-150$ days.

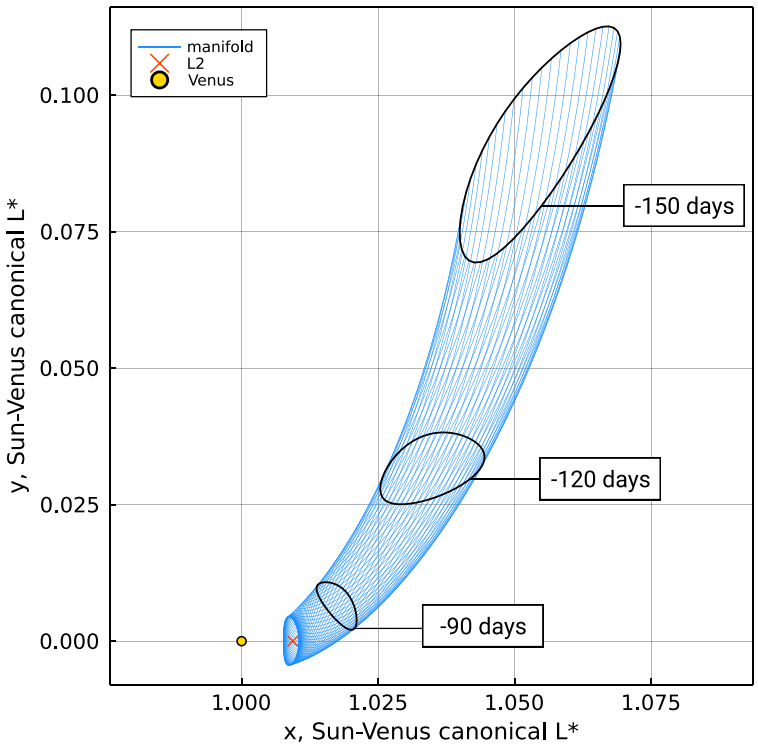


**Figure 7. Stable manifold and Poincare-Sections $\Gamma$ corresponding to $\Delta t_{\text{manifold}} = -90, -120$, and $-150$ days**

### Comparison of Global Optimal Solutions for Fixed and Free Poincaré Sections

The fixed-PS arrival is studied using $\Delta t_{\text{manifold}}$ at $-90$, $-120$, and $-150$ days along the stable manifold, and are denoted as cases I, II, and III. The free-PS arrival is studied using $\Delta t^{\text{min}}_{\text{manifold}} = -90$ days and $\Delta t^{\text{max}}_{\text{manifold}} = -150$ days, and is denoted as case IV. Table 4 summarizes the information of the best solution found for each case using MBH, and the corresponding trajectories are shown in Figure 8 in the ECLIPJ2000 frame, and specifically, the final portions captured in the manifold are shown in Figure 9 in the Sun-Venus CR3BP frame.

The optimal insertion point into the manifold is found from case IV to be $\Delta t_{\text{manifold}} \approx -120.44$ days, falling extremely close to case II. This is in agreement with the results from cases I through III, where the best final mass ratio is found for $\Delta t_{\text{manifold}} = -120$ days. The insertion angle parameter $\phi$ is found to be optimal at $\phi \approx 0.33$ in all four cases. Comparing the four cases, it is evident that the best trajectories belong to the same family of solutions with regards to the alignments of Earth and the Sun-Venus system, as they share the same launch epoch, fly-by epoch, and epoch at which they arrive at the LPO. The insertion epoch to the PS vary since each case spends a different duration in the manifold, but as expected cases II and IV have the same insertion epoch to the PS as well, since the duration they spend in the manifold is approximately the same. This is also visible from comparing the trajectory in Figures 8 and 9, as well as the history of the throttle $\tau$ shown in Figure 10. Even for the fixed PS cases, the global trajectory remains the same, irrespective of the insertion point. However, this comes at a cost in the final mass ratio, albeit within

**Table 4. Best result from Monotonic Basin Hopping**

| Case | I | II | III | IV |
|---|---|---|---|---|
| PS type | fixed | fixed | fixed | free |
| $\Delta t^{\text{min}}_{\text{manifold}}$, days | $-90$ | $-120$ | $-150$ | $-90$ |
| $\Delta t^{\text{max}}_{\text{manifold}}$, days | $-90$ | $-120$ | $-150$ | $-150$ |
| Launch date, UTC | 2023-05-14 20:33:40.456 | 2023-05-12 20:31:17.462 | 2023-05-09 11:33:56.892 | 2023-05-13 07:11:31.103 |
| Fly-by date, UTC | 2024-06-07 23:07:38.023 | 2024-06-04 08:07:11.788 | 2024-06-04 01:14:10.313 | 2024-06-04 14:51:27.732 |
| Arrival to PS, UTC | 2026-02-14 14:33:39.802 | 2026-01-12 14:31:18.392 | 2025-12-10 05:33:57.819 | 2026-01-12 14:34:54.782 |
| Arrival to LPO, UTC | 2026-05-15 14:33:39.802 | 2026-05-12 14:31:18.391 | 2026-05-09 05:33:57.817 | 2026-05-13 01:11:31.517 |
| Launch $\Delta v_\infty$, $\mathrm{km/s}$ | 1.5000 | 1.5000 | 1.5000 | 1.5000 |
| Fly-by $\Delta v_\infty$, $\mathrm{km/s}$ | 2.4287 | 2.5058 | 2.4844 | 2.4925 |
| $\phi$ | 0.32610 | 0.32530 | 0.32253 | 0.32557 |
| Optimal $\Delta t_{\text{manifold}}$, days | - | - | - | -120.442092 |
| Total time of flight, year | 3.00000 | 3.00000 | 3.00000 | 3.00000 |
| Final mass ratio | 0.91439 | 0.91488 | 0.91480 | 0.91494 |

3% of the best final mass ratio found from case IV. Finally, in all cases, it is possible to observe that the plane change is done through the fly-by, which is expected behavior for the global optimal solution as plane-change maneuvers are expensive otherwise.

**Analysis of Solution Space**

Figure 11 shows the distribution of key problem variables for all feasible solutions found for each case. It is possible to observe spikes in launch windows and times of flight, corresponding to favorable phasing for the interplanetary transfer sequence. With respect to the insertion point along the PS, the $\phi$ parameter is mostly concentrated at $\phi \approx 0.33$, suggesting that this insertion point into the manifold allows for a smooth connection from the interplanetary portion of the transfer. The spike in $\phi$ slightly shifts to larger values from case I to case III, suggesting that depending on the insertion epoch, the range of optimal insertion locations into the manifold shifts. The smaller spike at $\phi = 1$ is an artifact of gradient-based optimization. Since $\phi$ is a periodic variable, the gradient-based optimizer may attempt to drive its value across the upper bound; assuming the optimal value is $\phi = 0.3$, the optimizer would attempt to increase $\phi$ if $\phi > 0.8$. For the time of flight, among cases I, II, and III, the range of feasible values diminish; this is due to the longer time spent on the manifold, which becomes increasingly restrictive to the time of flight budget. Comparatively, since in case IV the optimizer is allowed to spend as little time on the manifold as in case I, a similar distribution of feasible time of flight is observed between cases I and IV.

For case IV, Figure 12 shows the distribution of $\Delta t_{\text{manifold}}$ for the feasible solutions. The largest spike exists at $\Delta t_{\text{manifold}} = -90$ days, where the trajectory spends the minimum amount of time on the manifold. Correspondingly, this allows for the longest amount of time left for the optimizer to use for the inter-system portion. This results in

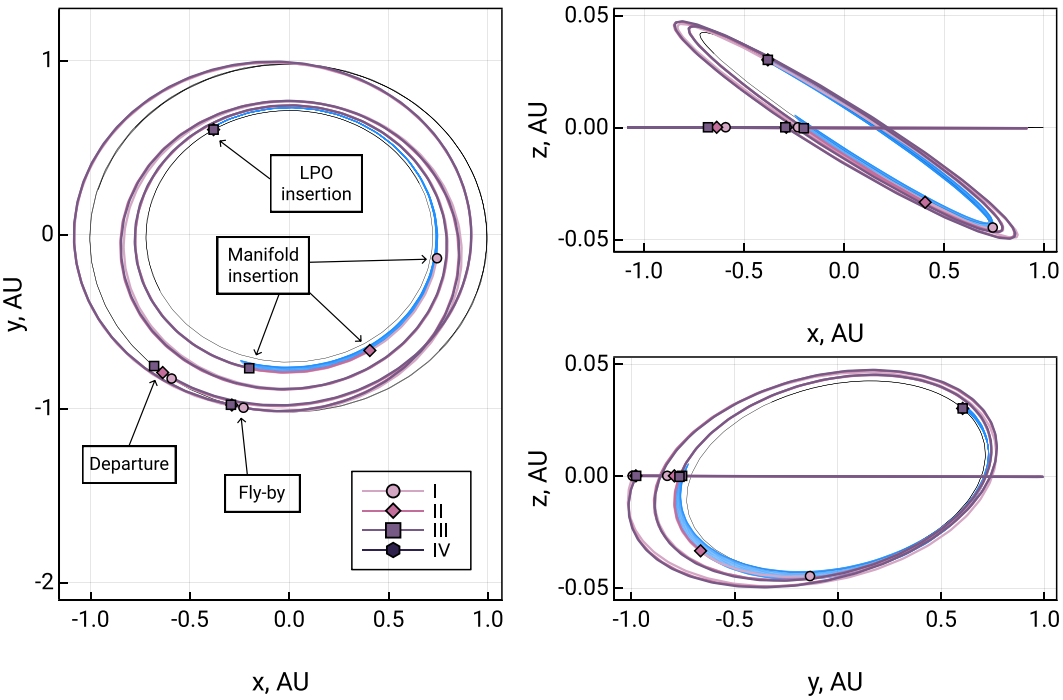


**Figure 8. Earth ∼ Earth ∼ Sun-Venus L2 LPO trajectory in ECLIPJ2000 of best solutions of cases I through IV with MBH search**

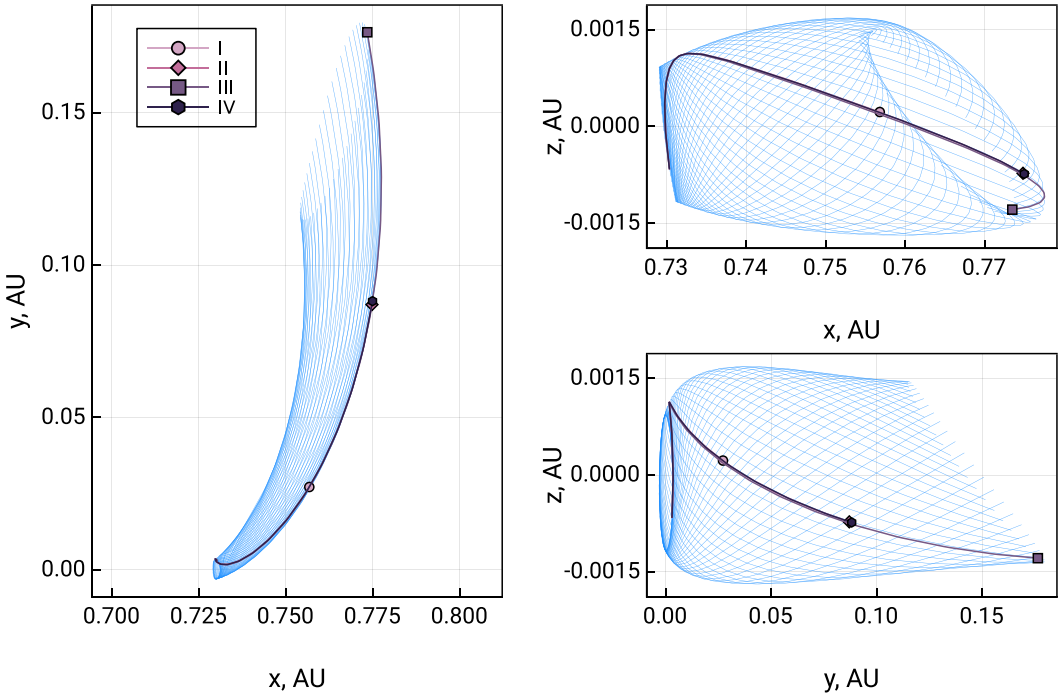


**Figure 9. Sun-Venus system portion of best solutions of cases I through IV with from MBH search**

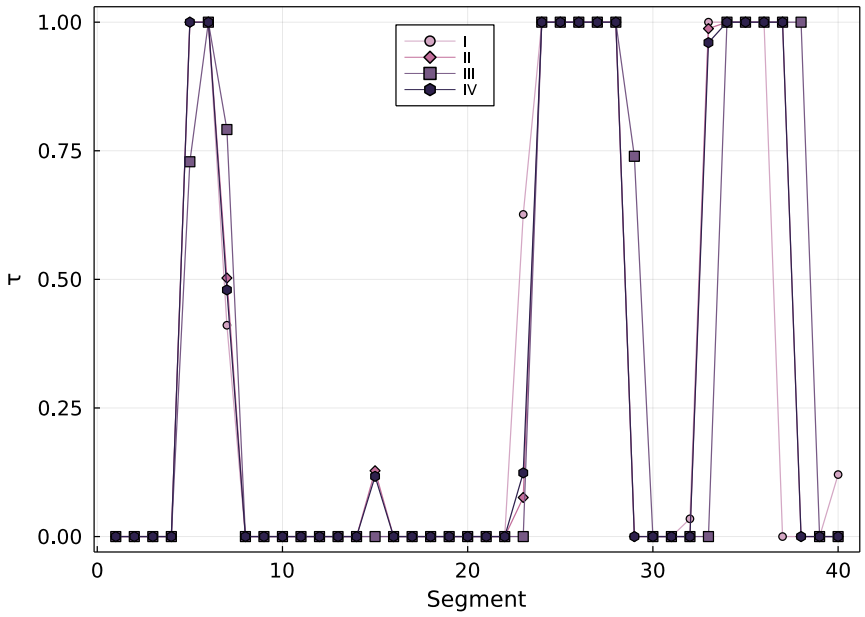


**Figure 10. Throttle histories of best solutions of cases I through IV with from MBH search**

maximum controllable duration where the thruster may be used for the longest time, thus resulting in a large number of feasible solutions. The smaller spike at $\Delta t_{\text{manifold}} \approx -120$ days corresponds to the region around the global optimal with respect to the insertion time. Finally, the other smaller spike at $\Delta t_{\text{manifold}} = -150$ days is the region where the trajectory spends the longest amount of time on the manifold. While this results in the minimum controllable duration, this directly translates to the minimum duration of potential mass expenditure as well. Since the objective is to maximize the final mass, it is reasonable that one type of locally optimal solutions exist where the longest amount of time is spent on the manifold, where no mass expenditure occurs.

## CONCLUSION

This work introduces a novel approach for designing gravity-assist low-thrust trajectories between systems, leveraging manifold captures to LPOs. The proposed method leverages the SFT, which provides an effective method for preliminary design of interplanetary trajectories with fly-by's. The modification is introduced at the definition of the nodes, where the trajectory inserts into an invariant manifold that leads to a LPO. Two formulations, one based on fixing a PS with a propagation time, and another where the optimizer chooses the location of the PS within some bounds on propagation time, are proposed. This framework is applied to study a transfer to a Sun-Venus L2 halo orbit, leveraging an Earth gravity-assist after launch. The results highlight the optimal manifold insertion location in state-space, a metric that has been previously unobtainable. The fixed PS-based formulation reveals insights into the problem structure, where the global optimal trajectory is found to be similar regardless of the insertion time into the manifold. The free PS-based formulation provides further information by identifying regions in the solution space

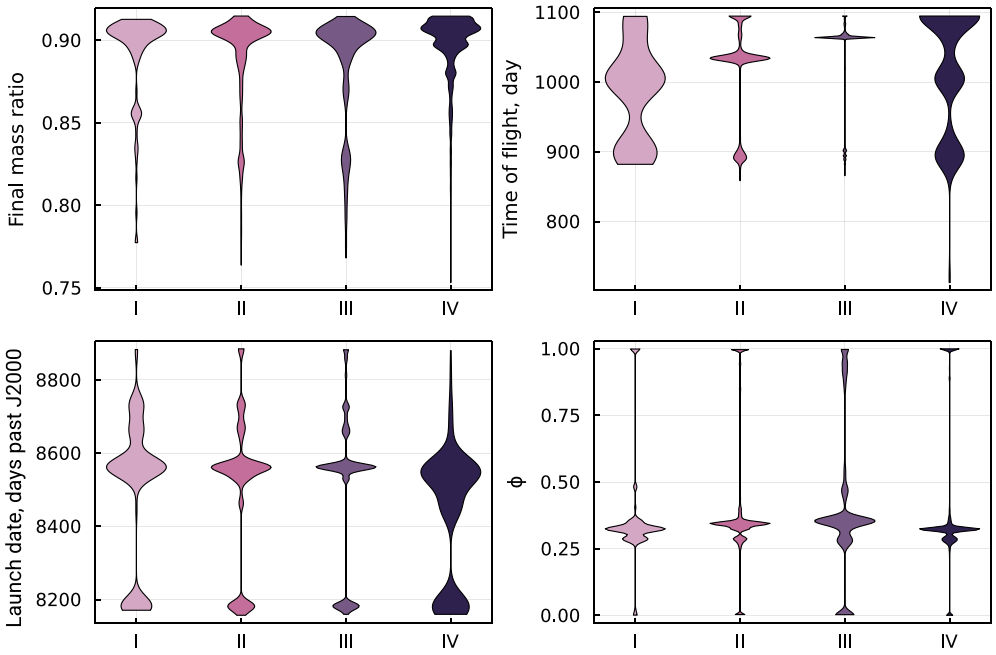


**Figure 11. Distribution of key variables of feasible solutions from cases I through IV**

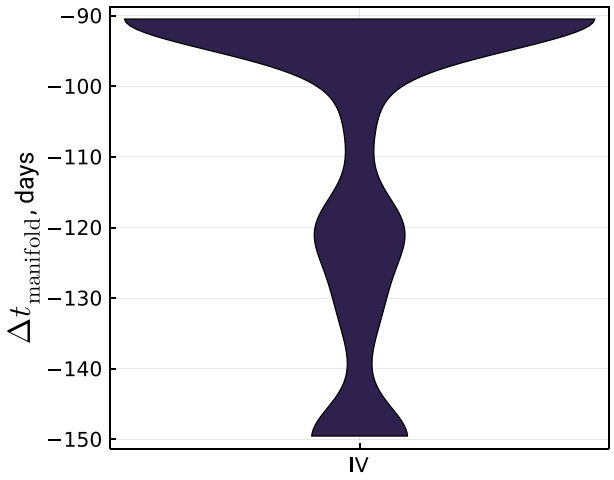


**Figure 12. Distribution of $\Delta t_{\mathrm{manifold}}$ of feasible solutions from case IV**

where the insertion time into the manifold is locally optimal. Overall, the approach presented in this work lays out the necessary strategy for designing preliminary interplanetary transfers that arrives to a LPO and assessing the feasible solution space.

As both crewed and robotic deep-space exploration missions are expected to increase in decades to come, end-to-end electric-propulsion-compatible transfer designs will become a key enabling strategy in sending large payloads. The method introduced in this work is capable of providing such transfers, enabling more demanding space missions and campaigns to be conducted.

## APPENDIX: ALGORITHM FOR LOW-THRUST APPROXIMATION VIA SUCCESSIVE IMPULSES IN TWO-BODY SYSTEM

Algorithm 3 is used for propagating the state-vector in the inter-system portion.

**Algorithm 3** Low-Thrust leg propagation via $n$ impulsive approximation

**Require:** $n > 0$, $\boldsymbol{r}_0$, $\boldsymbol{v}_0$, TOF
  **for** $i = 1$ to $n + 1$ **do**
    **if** $i = 1$ **then**
      $[\boldsymbol{r}_1, \boldsymbol{v}_1] \leftarrow \texttt{propagate}(\boldsymbol{r}_0, \boldsymbol{v}_0, t = \frac{\text{TOF}}{2n})$ ▷ propagate trajectory by $t = \frac{\text{TOF}}{2n}$ via equations (1) and (2)
      $\boldsymbol{v}_1 \leftarrow \boldsymbol{v}_1 + \Delta\boldsymbol{v}_i$ ▷ apply impulsive $\Delta v$
      $m_1 \leftarrow m_0 - \Delta m$ ▷ update spacecraft mass
    **else if** $i \neq n + 1$ **then**
      $[\boldsymbol{r}_1, \boldsymbol{v}_1] \leftarrow \texttt{propagate}(\boldsymbol{r}_0, \boldsymbol{v}_0, t = \frac{\text{TOF}}{n})$ ▷ propagate trajectory by $t = \frac{\text{TOF}}{n}$ via equations (1) and (2)
      $\boldsymbol{v}_1 \leftarrow \boldsymbol{v}_1 + \Delta\boldsymbol{v}_i$ ▷ apply impulsive $\Delta v$
      $m_1 \leftarrow m_0 - \Delta m$ ▷ update spacecraft mass
    **else**
      $[\boldsymbol{r}_1, \boldsymbol{v}_1] \leftarrow \texttt{propagate}(\boldsymbol{r}_0, \boldsymbol{v}_0, t = \frac{\text{TOF}}{2n})$ ▷ propagate trajectory by $t = \frac{\text{TOF}}{2n}$ via equations (1) and (2)
    **end if**
    $\boldsymbol{r}_0 \leftarrow \boldsymbol{r}_1$
    $\boldsymbol{v}_0 \leftarrow \boldsymbol{v}_1$
  **end for**

## CONFLICT OF INTEREST

On behalf of all authors, the corresponding author states that there is no conflict of interest.

## REFERENCES


[1] S. D. Ross, "The interplanetary transport network," *American Scientist*, Vol. 94, No. 3, 2006, pp. 230–237, 10.1511/2006.59.994.

[2] W. S. Koon, M. W. Lo, J. E. Marsden, and S. D. Ross, *Dynamical Systems, the Three-Body Problem and Space Mission Design*. 2011.

[3] F. Topputo, M. Vasile, and F. Bernelli-Zazzera, "Interplanetary and lunar transfers using libration points," *European Space Agency, (Special Publication) ESA SP*, No. 548, 2004, pp. 583–588.

[4] R. T. Eapen and R. K. Sharma, "Mars interplanetary trajectory design via Lagrangian points," *Astrophysics and Space Science*, Vol. 353, No. 1, 2014, pp. 65–71, 10.1007/s10509-014-2012-x.

[5] F. Topputo and E. Belbruno, "Earth–Mars transfers with ballistic capture," *Celestial Mechanics and Dynamical Astronomy*, Vol. 121, No. 4, 2015, pp. 329–346, 10.1007/s10569-015-9605-8.

[6] D. Canales, K. C. Howell, and E. Fantino, "Transfer design between neighborhoods of planetary moons in the circular restricted three-body problem: the moon-to-moon analytical transfer method," *Celestial Mechanics and Dynamical Astronomy*, Vol. 133, No. 8, 2021, pp. 1–44, 10.1007/s10569-021-10031-x.

[7] H. Pernicka, D. Henry, and M. Chan, "Use of halo orbits to provide a communication link between earth and Mars," *AIAA/AAS Astrodynamics Conference*, 1992, pp. 445–455, https://doi.org/10.2514/6.1992-4585.

[8] J. D. Strizzi, J. M. Kutrieb, P. E. Damphousse, and J. P. Carrico, "Sun-Mars libration points and Mars mission simulations," *AAS/AIAA Astrodynamics Specialist Conference*, 2001, pp. 807–822.

[9] M. Shirobokov, S. Trofimov, and M. Ovchinnikov, "On the design of a space telescope orbit around the Sun–Venus L2 point," *Advances in Space Research*, Vol. 65, No. 6, 2020, pp. 1591–1606, 10.1016/j.asr.2019.12.022.

[10] I. D. Kovalenko, N. A. Eismont, S. S. Limaye, L. V. Zasova, D. A. Gorinov, and A. V. Simonov, "Micro-spacecraft in Sun-Venus Lagrange point orbit for the Venera-D mission," *Advances in Space Research*, Vol. 66, No. 1, 2020, pp. 21–28, 10.1016/j.asr.2019.10.027.

[11] D. Senske, L. Zasova, A. Burdanov, T. Economou, N. Eismont, M. Gerasimov, D. Gorinov, J. Hall, N. Ignatiev, M. Ivanov, K. Lea Jessup, I. Khatuntsev, O. Korablev, T. Kremic, S. Limaye, I. Lomakin, M. Martynov, A. Ocampo, S. Teselkin, O. Vaisberg, and V. Voronstsov, "Development of the Venera-D Mission Concept, from Science Objectives to Mission Architecture," *49th Lunar and Planetary Science Conference*, 2018.

[12] Y. Tanaka, Y. Kawakatsu, and H. Yoshimura, "Design of Escaping Trajectory from Mars by Using a Halo Orbit as Hub and a Method of Delta V Reduction," *The 28th Workshop on JAXA Astrodynamics and Flight Mechanics*, 2018, pp. 3–8.

[13] J. A. Sims and N. Flanagan, "Preliminary design of low-thrust interplanetary missions," *AAS Astrodynamics Specialists Conference*, 1999.

[14] J. A. Sims, P. A. Finlayson, E. A. Rinderle, M. A. Vavrina, and T. D. Kowalkowski, "Implementation of a low-thrust trajectory optimization algorithm for preliminary design," *AIAA/AAS Astrodynamics Specialist Conference*, 2006, 10.2514/6.2006-6746.

[15] T. T. McConaghy, T. J. Debban, A. E. Petropoulos, and J. M. Longuski, "Design and optimization of low-thrust trajectories with gravity assists," *Journal of Spacecraft and Rockets*, Vol. 40, No. 3, 2003, pp. 380–387, 10.2514/2.3973.

[16] C. H. Yam, T. T. McConaghy, K. J. Chen, and J. M. Longuski, "Design of low-thrust gravity-assist trajectories to the outer planets," *International Astronautical Federation - 55th International Astronautical Congress 2004*, Vol. 1, 2004, pp. 476–491, 10.2514/6.iac-04-a.6.02.

[17] C. H. Yam, D. Izzo, and D. D. Lorenzo, "Low-thrust trajectory design as a constrained global optimization problem," *Proceedings of the Institution of Mechanical Engineers, Part G: Journal of Aerospace Engineering*, Vol. 225, No. 11, 2011, pp. 1243–1251, 10.1177/0954410011401686.

[18] C. H. Yam, D. Izzo, and F. Biscani, "Towards a High Fidelity Direct Transcription Method for Optimisation of Low-Thrust Trajectories," *4th International Conference on Astrodynamics Tools and Techniques.*, 2010, pp. 1–7.

[19] R. R. Bate, D. D. Mueller, and J. E. White, *Fundamentals of Astrodynamics*. New York: Dover Publications, 1971.

[20] D. L. Richardson, "Analytic construction of periodic orbits about the collinear points," *Celestial Mechanics*, Vol. 22, No. 3, 1979, pp. 241–253, 10.1007/BF01229511.

[21] K. C. Howell, "Three-Dimensional, Periodic, Halo Orbits," *Celestial Mechanics*, Vol. 32, No. 53, 1984.

[22] Y. Shimane and K. Ho, "Robustness Assessment of Low-Thrust Trajectory via Sequentially Truncated Sims-Flanagan Problems," *AIAA ASCEND*, Las Vegas, 2021, pp. 1–16, 10.2514/6.2021-4153.

[23] B. A. Conway, "An Improved Algorithm Due to Laguerre for the Solution of Kepler's Equation," *Celestial Mechanics*, Vol. 39, No. 1980, 1986, pp. 199–211.

[24] G. J. Der, "An elegant state transition matrix," *The Journal of Astronautical Sciences*, Vol. 45, No. 4, 1996, pp. 776–791, 10.2514/6.1996-3660.

[25] J. A. Englander and A. C. Englander, "Tuning Monotonic Basin Hopping: Improving the Efficiency of Stochastic Search as Applied to Low-Thrust Trajectory Optimization," *International Symposium on Space Flight Dynamics*, 2014, pp. 1–33.

[26] J. A. Englander, J. M. Knittel, K. Williams, D. Stanbridge, and D. H. Ellison, "Validation of a low-thrust mission design tool using operational navigation software," *AAS/AIAA Space Flight Mechanics Meeting*, Vol. 160, 2017, pp. 3899–3918.

[27] P. E. Gill, W. Murray, and M. A. Saunders, "SNOPT: An SQP algorithm for large-scale constrained optimization," *SIAM Review*, Vol. 47, No. 1, 2005, pp. 99–131, 10.1137/S0036144504446096.

[28] A. Wächter and L. T. Biegler, "On the implementation of an interior-point filter line-search algorithm for large-scale nonlinear programming," *Mathematical Programming*, Vol. 106, No. 1, 2006, pp. 25–57, 10.1007/s10107-004-0559-y.

[29] D. J. Wales and J. Doye, "Global Optimization by Basin-Hopping and the Lowest Energy Structures of Lennard-Jones Clusters Containing up to 110 Atoms," *The Journal of Physical Chemistry A.*, Vol. 101, No. 28, 1997, pp. 5111–5116.

[30] D. Izzo, "PyGMO and PyKEP: open source tools for massively parallel optimization in astrodynamics (the case of interplanetary trajectory optimization)," *5th International Conference Astrodynamics Tools and Techniques*, 2012.

[31] S. L. McCarty and M. L. McGuire, "Parallel monotonic basin hopping for low thrust trajectory optimization," *Space Flight Mechanics Meeting, 2018*, No. 210009, 2018, 10.2514/6.2018-1452.